A MAGNETIC FORCE DRIVEN CHAOTIC MICRO-MIXER

Hiroaki Suzuki
Department of Mechanical Engineering, The University of Tokyo
7-3-1, Hongo, Bunkyo-ku, Tokyo 113-8656, Japan

Chih-Ming Ho
Mechanical & Aerospace Engineering Department, University of California,
Los Angeles, USA 90095-1597

ABSTRACT

A magnetic force based chaotic micro-mixer is developed for mixing of magnetic beads in bio-fluids. The mixer consists of micro-conductors embedded in the substrate and micro-channel on top. We have shown that the magnetic field generated by the simple 2-D micro-conductors provides strong attraction to the nearby magnetic beads. Numerical simulation was used to search for the chaotic regime of particle trajectories. It is found that the serpentine channel geometry with the perpendicular electrodes arrangement is able to create the stretching and folding of material lines, which is a sign of chaos. The existence of chaos is also verified by using the dynamical tools, such as Lyapunov exponent and Poincaré map.

INTRODUCTION

In molecular biology studies, magnetic beads (spherical polymer micro-particles containing iron oxide) coated with ligand or antibody are commonly used for selective separation of biomolecules from the mixture [1-4]. When the magnetic beads are added to complex biomolecule mixture, beads and target molecule bind together to form a beads-target complex (target is labeled). Eventually, the magnetically labeled molecules are separated by applying strong magnetic field. Miniaturization of this separation system will offer many advantages over the existing bench-top protocols, such as compact size, gentle and fast separation, and extremely small sample volume (Fig. 1).

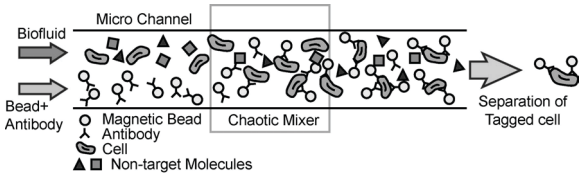

Fig. 1 Schematic diagram of the magnetic separation of biomolecules in the micro-device.

In such a micro-fluidic devices, mixing becomes a serious problem [5-8] due to the extremely low Reynolds number (Re < 1). Molecular diffusion is the only possible mechanism, since turbulence is not available. Diffusion is governed by Fick's law, $J = -D \cdot \partial C / \partial x$, where J is diffusive mass flux and C is concentration. D is diffusion coefficient based on Brownian motion, which is written as

$$D = \frac{\kappa T}{6\pi\mu d_p},$$

where κ is Voltzman constant, T is absolute temperature of the fluid, d_p is diameter of particle, and μ is the dynamic viscosity of the fluid. The time constant of the diffusion τ_D is written as

$$\tau_D = \frac{L^2}{D},$$

where L is the characteristic length (e.g. channel width).

Typically, D of water-soluble molecules, such as iron and dye, is on the order of 10^{-9} [m^2/s]. In this case, τ_D is 10 second to diffuse the distance L of 100 μm. However, diffusion of larger particles such as biomolecules and magnetic beads becomes more inefficient since their diameter is much larger. For the molecules of 1~10 μm, τ_D becomes 10^2~10^3 seconds, which is too long and impractical.

On the other hand, chaotic motion is an interesting way of achieving mixing [9, 10]. While chaos in turbulence (dissipative system) is called Eulerian Chaos, that in laminar flow (conservative system) is called Lagrangian chaos. A state of Lagrangian chaos is recognized as a system in which the trajectory equations have a sensitive dependence on initial conditions, and initially nearby trajectories diverge exponentially fast. Thus, the solutions eventually enter the unpredictable state. It is also known that the stretching and folding of material element is the sign of chaos.

With the aid of chaos theory, it can be possible to achieve an efficient mixing in the very low Reynolds number flow. In this paper, chaotic mixing of magnetic beads in the micro-channel is explored by applying local time-varying magnetic force to facilitate the mixing and to enhance the attachment of beads to biomolecules. Firstly, a simple straight channel and electrodes are fabricated, and its magnetic field was examined for determining whether the field is strong enough to drive the magnetic beads. Then, the design of the channel, electrodes, and driving signal, which is able to generate chaos, is examined by numerical simulation. Numerical results will be used for the next generation of chaotic micro-mixer.

BASIC DESIGN AND FABRICATION

The magnetic micro-mixer in this study consists of micro-conductors embedded in the substrate and a micro-channel formed as a mixer (Fig. 2a). The channel has two inlets and one

outlet from the backside. When the current is applied to a pair of parallel conductors located in the mixing region, magnetic field is generated (Fig. 2b) so that the magnetic beads are attracted toward the center of two conductors.

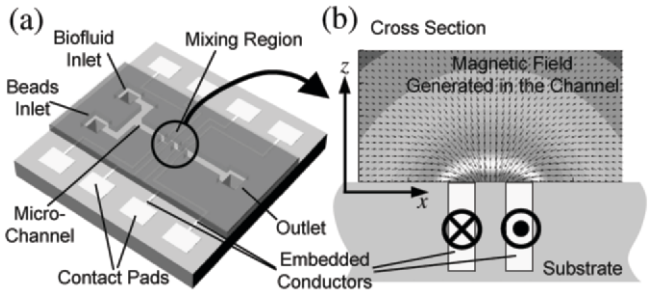

Fig. 2 (a) Schematic view of the magnetic micro-mixer. (b) Sectional view of mixing region. When current is applied to a pair of embedded conductors, magnetic field is generated.

The fabrication process is shown in Fig. 3. After the oxidation and nitride deposition, fluid inlet/outlet holes are opened by KOH etching from the backside. Then, the pattern of electrode is defined on the front side and etched with deep RIE down to 60μm. The photoresist is left for the next liftoff process. Ti/Cu seed layer is deposited and lifted off so that it remains only in the recessed area. Then, copper is electroplated to fill up the trenches, followed by planarization. With this method, embedded conductor with the large sectional area is achieved, which allows relatively large current (up to 1A). Also, the resulting planar surface allows the further fabrication of structure on the substrate, so that the wafer bonding can be avoided. After the insulation of the surface, micro-channel is patterned and fabricated with SU-8 photoresist. Then, a thin cover glass is bonded on top to close the channel. To avoid the biological contamination, PEG (polyethylene glycol)[11] is applied to inside wall of the channel. Finally, inlet/outlet tubes are bonded with epoxy from the backside.

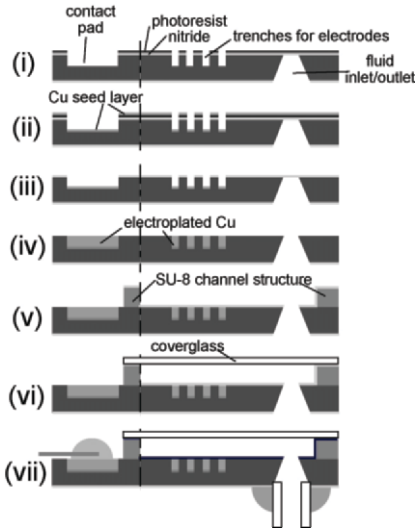

Fig. 3 Fabrication Process. (i) After backside KOH etching for fluid inlet and outlet, the pattern of electrodes are defined and etched with Deep RIE. (ii) Seed layer deposition. (iii) Liftoff. (iv) Copper electroplating followed by planarization. (v) Channel is formed by SU-8, and PECVD oxide is deposited. (vi) Coverglass is bonded to close the channel. (vii) Packaging (tubing, soldering).

CHARACTERIZATION

Fig. 4 shows microscope images of magnetic beads (d_p = 1 μm, Spherotech, Inc., CM-10-10) suspended in water are flowing in the straight channel (200μm in width and 30μm in height) from left to right. Approximate flow rate is 0.6 nL/s. Conductor line width and intervals are both 20μm. When 500 mA current is applied to conductors 1 and 2, beads are attracted and captured in their center region (Fig. 4a). Thus, it is shown that the simple geometry coil is able to immobilize the magnetic beads. When turned off, they are released and flow to the downstream (Fig. 4b).

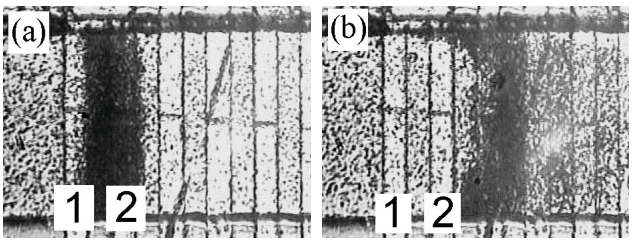

Fig. 4 Microscope images. (a) Beads are trapped between two conductors. (b) Beads are released when current is turned off.

To estimate the magnetic force on beads, 2-D magnetic field around the two infinite-long parallel conductors is numerically calculated by integrating Biot-Savart law (see Fig. 2b). Given the magnetic field $\boldsymbol{H}$, magnetic force $\boldsymbol{F}_m$ on beads is estimated by

$$\boldsymbol{F}_m = (1 - N_d)\chi V_m (\boldsymbol{H} \cdot \nabla)\boldsymbol{B} ,$$

where N_d is a demagnetizing factor (0.333 for a sphere), χ is susceptibility, V_m is volume of magnetic material, $\boldsymbol{B}$ is magnetic induction ($\boldsymbol{B} = \mu_0 \boldsymbol{H}$). Susceptibility χ (= 3.0) is measured by VSM (Vibrating Sample Magnetometer). Then, velocity of beads in water $\boldsymbol{v}_p$ is derived from Stoke's drag equation,

$$\boldsymbol{F}_d = 3\pi\mu d_p \boldsymbol{v}_p .$$

Figure 5 shows the force and velocity of beads induced by DC magnetic field when current of 500 mA is applied. Conductors span at x = ±10 ~ ±30 μm and z = 0 ~ -60 μm. As expected, direction of F_m is toward the center of two conductors (x = 0). Magnetic force on the order of pico-newton is generated, and equilibrium velocity reaches few tens of microns per second.

To verify this calculation, the velocity of beads in the static water when DC magnetic field is applied is estimated from the flow visualization movie experimentally. Figure 5(b) shows experimental measurement and theoretical calculation at different z. The discrete distribution of experimental data is due to the resolution of visualization. Also, since all beads at different z location are captured in the images, velocity of beads spans in a

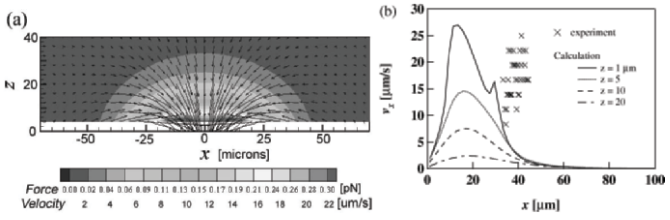

Fig. 5 (a) Force and velocity field around the two embedded conductors (20 × 60 μm, 20μm interval). (b) Velocity in x direction, experiment (markers) and theoretical calculation (lines).

wide range (8 ~ 25 mm/s). However, if compared at their medium value, the difference is about the factor of 5, and they are roughly on the same order. The difference might be due to the magnetic characteristics of beads, since the measurement of χ of the superparamagnetic particle is not trivial. Despite this difference, we can say that the magnitude of magnetic force and particle velocity is predicted, and now we are ready to calculate the motion of beads.

TWO DIMENSIONAL NUMERICAL SIMULATION OF CHAOTIC FLOW

Numerical simulation is used to facilitate the design of channel configuration and the choice of forcing signal that is able to create chaotic trajectories of beads. Since time-periodic 2-D flow has a chance of producing chaos [9, 10], particle trajectories in 2-D steady flow field perturbed by unsteady magnetic force are examined. The simulation is carried out as follows.

1. Design of Flow Configuration

In the past, numerous studies on Lagrangian Chaos had been done in 2-D closed flow (e.g., cavity flow, journal bearing flow) [9, 10]. However, it is still challenging to explore the chaos in open flow system, which is common in micro-fluidic systems.

In the recent studies in our group, chaotic mixing is created by pushing and pulling the elements between low and high velocity region, by using either pressure or DEP (dielectrophoretic) force [5-7]. Stretching and folding is induced by this way, and the corner of channel branch (side cavity) works as a saddle point (Fig. 6a). However, with the magnetic force, only attractive force can be achieved, so that elements (beads) attracted toward the low velocity region will not come back to the high velocity region (Fig. 6b).

To solve this problem, serpentine channel geometry with perpendicular coil arrangement (Fig. 7, one unit is 160×80 μm^2) is employed. This unit repeats in x direction. Driving signal and

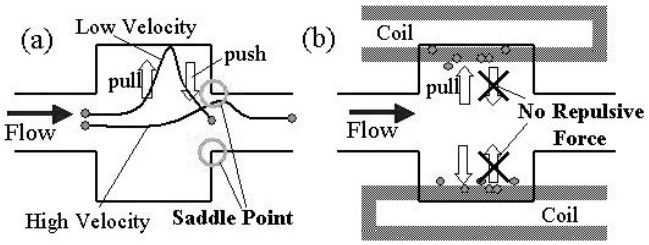

Fig. 6 (a) Strategy of creating chaos when both attractive and repulsive forces are available. (b) Particles will be stuck in the low velocity region without repulsive force.

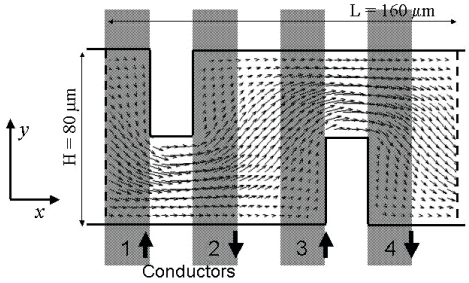

Fig. 7 2-D flow field in the serpentine channel and conductor arrangement (shaded area). This unit repeats in x direction.

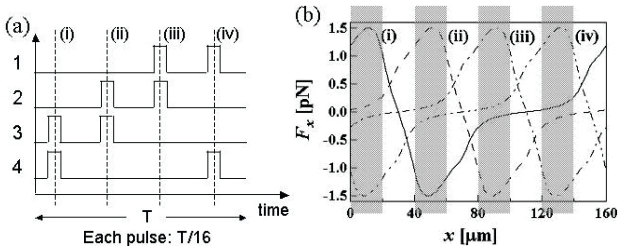

Fig. 8(a) Driving signal, (b) Magnetic force in x direction at each instant (i)~(iv).

magnetic force at each quarter period (i)~(iv) is shown in Fig. 8(a) and 8(b), respectively. For example, when the current is applied to conductor 1 and 2 (period iii) in the opposite direction, magnetic beads are attracted toward their center. The phase shift quarter period is given to each pair of conductors.

2. Numerical Scheme

Firstly, steady flow field in the serpentine channel with no disturbance is calculated by using commercial CFD code (CFDRC) as shown in Fig. 7. Then, based on this flow field, particle velocity is derived as a vector sum of local fluid velocity and the velocity due to the magnetic force. Particle trajectories are calculated by integrating the particle velocities with 4th order Runge-Kutta method. This scheme is valid when the particle response time is very small compared with the time-scale of flow field. Molecular diffusion is not considered. Averaged fluid velocity U is set to 40 μm/s ($Re_H = 3.2 \times 10^{-3}$). Flow pattern is investigated by changing two parameters, the maximum value of velocity induced by magnetic force (v_{max}/U) and driving frequency ($St_U = fH/U$).

3. Flow visualization

Figure 9 shows the deformation of the lump of 7800 particles initially located at the shaded area. When there is no disturbance, particles exactly follow the streamline and never be advected to the upper side of the channel (Fig. 9a). On the other hand, when the unsteady magnetic force shown in Fig. 8 is applied at v_{max}/U = 1.3 and St_U = 0.54, stretching and folding are induced, and particles are spread all over the channel after 4 periods of perturbation (Fig. 9b).

Fig. 10 (a)~(d) shows the successive images of lump of particles, showing the mechanism of stretching and folding. In Fig. (a) and (b), the electrodes 1 and 2 are turned on, and magnetic force attracts particles toward their center (small arrows in Fig. 10a). While particles in the lower velocity region are attracted toward the corner of the channel (arrow A in Fig. 10b), those in the higher velocity region remain be advected by the main flow (arrow B). Folding is induced in this way. As particles are further

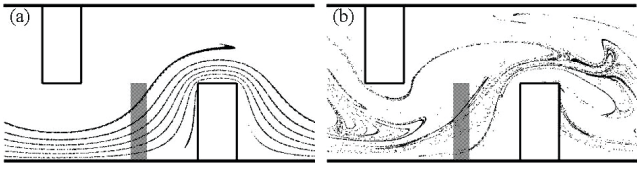

Fig. 9 Deformation of the lump of particles. (a) Without disturbance, (b) With the signal shown in Fig. 8.

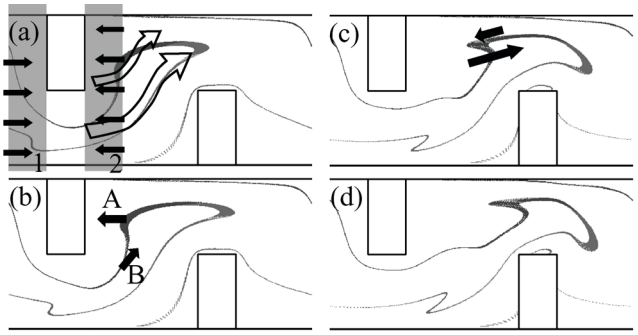

Fig 10 Successive images of lump deformation.

advected downstream, the fold is stretched by the shear (arrows in Fig. 10c).

4. Analysis

Dynamical tools are used to verify the existence of chaos [9, 10]. Poincaré map, which is the plot of the position of particles at each forcing period, displays in a single plot the character of the system by reducing the number of dimensions. Figure 11 shows the Poincaré maps of 7 particles evenly distributed in *y* direction initially. Without the perturbation, the mapping is regular (Fig. 11a). However, when perturbed with the same signal as Fig. 9(b), it becomes spreading all over the channel (Fig. 11b).

To characterize chaos quantitatively, Lyapunov exponent σ (hereafter, LE), which is an index of the divergence of initial condition, is calculated as,

$$\sigma = \lim_{\substack{t\to\infty \\ |dX|\to 0}} \left[\frac{1}{t} \ln\left(\frac{|dx|}{|dX|} \right) \right],$$

where $|dX|$ is the length of a vector of initial condition dX, and $|dx|$ is its length at time t. If σ is positive non-zero number, then

$$|dx| \approx |dX| \exp(\sigma t)$$

and the distance of two initially nearby particles diverges exponentially with time. In chaos studies, infinite-time LE, which is a long time average of stretching rate, is often used. However, in mixing problems, short time behavior should be examined, since we need mixing as fast as possible. For this purpose, finite-time time LE, which is the average of LE of many particles for the short time (in our case, 4 cycles of forcing).

Fig. 12 shows the infinite and finite time LE at different St_U and v_{max}, respectively. In Fig. 12(a), both exponents coincide, and they are positive, which indicates the exponential divergence of initially nearby particles, over the wide range of forcing Strouhal number. The optimum frequency exists around St_U = 0.4~0.6 for driving the flow toward chaos. In Fig. 12(b), both exponents are also positive over the wide range of v_{max}/U. They increase as the magnitude of perturbation become larger until v_{max}/U ~ 2.8, then dramatically drop down. The fluctuation of infinite-time LE around v_{max}/U ~ 1.6 is because all the particles fall into one trajectory and LE became unstable in a long term, which does not happen in a short time. With the parameters showing large exponents, stretching and folding mechanism shown in Fig. 10 is produced. In this system, the matching of the driving frequency and the flow time constant facilitates the stretching and folding of the material lines.

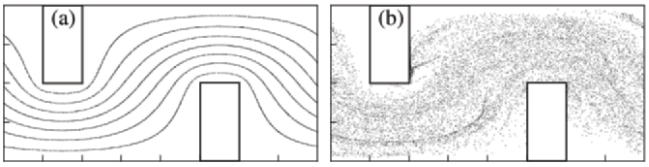

Fig. 11 Poincaré maps (a) without, (b) with perturbation.

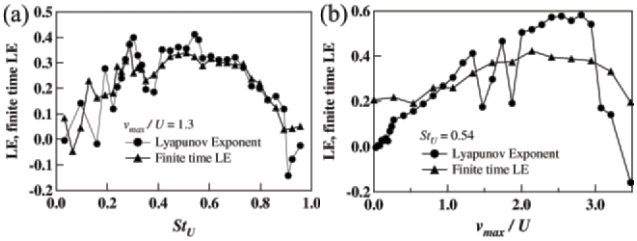

Fig. 12 Infinite and finite time Lyapunov exponent. (a) Frequency and (b) amplitude dependence.

CONCLUSIONS

The prototype of magnetic force based micro-mixer, which consists of embedded micro-conductors and micro-channel, is fabricated. It is shown that the simple 2-D micro-conductors are able to generate enough magnetic force to attract the nearby magnetic beads. Numerical simulation is carried out to find the flow system that can produce chaotic motion by tracing particles in Lagrangian manner. The serpentine channel geometry with the perpendicular electrode arrangement is shown to be able to create the stretching and folding of material lines, which is a sign of chaos. Optimum forcing frequency was found and lies in a wide range. In this system, the matching of the driving frequency and the flow time constant facilitates the excellent mixing.

REFERENCES

[1] B. Sinclair, "To Bead or Not To Bead: Applications of Magnetic Bead Technology," The Scientist, Vol. 12, No. 13 (1998).

[2] M. Zborowski et al., "Continuous cell separation using novel magnetic quadrupole flow sorter," J. Magnetism and Magnetic Materials, 194, pp. 224-230 (1999).

[3] J. W. Choi et al., "A New Magnetic Bead-Based, Filterless Bio-Separator with Planar Electromagnet Surfaces for Integrated Bio-Detection Systems," Sensors and Actuators, B 68, pp. 34-39 (2000).

[4] J. W. Choi et al., "An Integrated Microfluidic Biochemical Detection System with Magnetic Bead-Based Sampling and Analysis Capabilities", Proc. MEMS Conf. 2001, pp. 447-450.

[5] C. M. Ho, "Fluidics - The Link between Micro and Nano Sciences and Technologies -," Proc. MEMS 2001, pp. 375-384.

[6] Y. K. Lee et al., "Characterization of a MEMS-Fabricated Mixing Device," ASME IMECE (2000).

[7] Y. K. Lee et al., "Chaotic Mixing in Electrokinetically and Pressure Driven Micro Flows," Proc. MEMS Conf. 2001, pp. 483-486.

[8] R. H. Liu et al., "Passive Mixing in a Three-Dimensional Serpentine Microchannel," J. MEMS, Vol. 9, No. 2, pp. 190-197 (2000).

[9] J. M. Ottino, "The Kinematics of Mixing: Stretching, Chaos, and Transport," Cambridge Univ. Press (1989).

[10] J. M. Ottino, "Mixing, Chaotic Advection, and Turbulence," Annu. Rev. Fluid Mech., 22, pp. 207-253 (1990).

[11] N. A. Alcantar et al., "Polyethylene Glycol-Coated Biocompatible Surfaces," J. Biomedical Materials Research, Vol. 51(3), 343-351 (2000).